Science of the Total Environment 647 (2019) 708–715

Contents lists available at ScienceDirect

Science of the Total Environment

journal homepage: www.elsevier.com/locate/scitotenv

Heteroaggregation and sedimentation of graphene oxide with hematite colloids: Influence of water constituents and impact on tetracycline adsorption

Yiping Feng [a,b,*], Khanh An Huynh [c], Zhijie Xie [a], Guoguang Liu [a], Shixiang Gao [b,**]

[a] Guangzhou Key Laboratory of Environmental Catalysis and Pollution Control, School of Environmental Science and Engineering, Institute of Environmental Health and Pollution Control, Guangdong University of Technology, Guangzhou, Guangdong 510006, China
[b] State Key Laboratory of Pollution Control and Resource Reuse, School of the Environment, Nanjing University, Nanjing, Jiangsu 210023, China
[c] Faculty of Environment and Natural Resources, Ho Chi Minh City University of Technology, Ho Chi Minh City, Viet Nam

HIGHLIGHTS

- Favorable heteroaggregation and sedimentation occurred between oppositely charged GO and HemNP.
- NOMs suppressed the sedimentation of GO—HemNP heteroaggregates through various mechanisms.
- High ionic strength enhanced the heteroaggregation and sedimentation of GO—HemNP heteroaggregates.
- Elevated pH partially disaggregated the GO—HemNP heteroaggregates.
- Coexistence of HemNP greatly reduced the adsorption of tetracycline on GO.

GRAPHICAL ABSTRACT

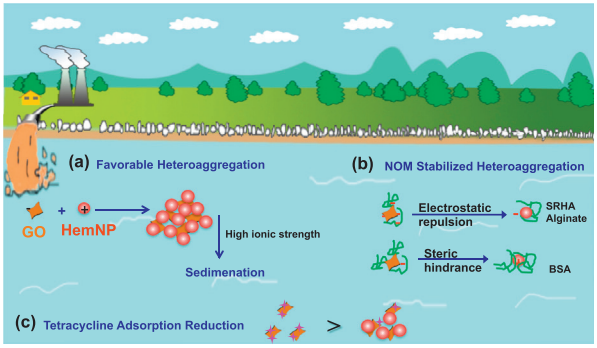

ARTICLE INFO

Article history:
Received 24 January 2018
Received in revised form 3 August 2018
Accepted 3 August 2018
Available online 5 August 2018

Editor: P Holden

Keywords:
Graphene oxide
Heteroaggregation
Sedimentation
Hematite
Natural organic matter

ABSTRACT

Because the transport of graphene oxide nanosheets (GO) from water to sediments is influenced by their heteroaggregation and sedimentation with natural colloids, knowledge on the interdependence of heteroaggregation and sedimentation for GO is needed to gain a better insight on the environmental fate of these nanosheets. However, this phenomenon is still not well understood. In this study, the heteroaggregation and sedimentation behaviors of GO with hematite nanoparticles (HemNPs) were investigated at various conditions. It has been found that negatively charged GO rapidly underwent heteroaggregation with positively charged HemNPs, leading to the sedimentation of GO. Significant sedimentation occurred when the net charge of the GO—HemNP mixture was close to zero. The presence of various natural organic matters suppressed the sedimentation of the heteroaggregates through various mechanisms. Specifically, adsorption of humic acid and alginate reversed HemNP surface charge from positive to negative, leading to a slow sedimentation of the GO—HemNP mixtures due to the increase in nanoparticle electrostatic repulsion. Adsorption of bovine serum albumin raised steric hindrance effect between GO and HemNP, which in turn inhibited their heteroaggregation and sedimentation. At high ionic strength conditions, the sedimentation of GO and HemNP was enhanced, possibly through the combination of homo- and hetero-aggregation. At elevated pH, the heteroaggregates were partially disaggregated, probably due to the weakening of GO—HemNP bonds as the surface charges of these nanomaterials became more negative. Moreover, heteroaggregation of GO with HemNP likely to occupy the adsorption sites on

* Corresponding author at: Guangzhou Key Laboratory of Environmental Catalysis and Pollution Control, School of Environmental Science and Engineering, Institute of Environmental Health and Pollution Control, Guangdong University of Technology, Guangzhou, Guangdong 510006, China.
** Corresponding author.
E-mail addresses: ypfeng@gdut.edu.cn (Y. Feng), ecsxg@nju.edu.cn (S. Gao).

https://doi.org/10.1016/j.scitotenv.2018.08.046

GO surfaces, thus greatly reduced the adsorption of tetracycline on GO. These findings highlighted the important roles of natural colloids on the fate and transport of GO, together with the importance of heteroaggregation on the adsorption of co-existing pollutants to GO in natural aquatic environments.

1. Introduction

Graphene oxide nanosheets (GO), which have a layered structure with oxygen-containing functional groups on the basal plane and the sheet edges, and can be used in the production of graphene or graphene-based composite materials (He et al., 1998; Kim et al., 2012; Zhu et al., 2010). As a result of worldwide commercial interests, GO and GO-based nanomaterials will be inevitably released into the environment during their production, transport, use, and disposal (Zhao et al., 2014). The potential environmental impacts of GO have raised significant concerns. Many investigations demonstrated that GO could induce toxic effects on bacteria and mammalian cells (Akhavan and Ghaderi, 2010; Bianco, 2013; Chang et al., 2011; Liao et al., 2011; Liu et al., 2011; Yang et al., 2013; Yang et al., 2010). Several studies have also found that the presence of GO amplified the toxicity of heavy metals to plant and algae (Hu et al., 2014; Tang et al., 2015).

Natural colloids, such as metal oxide particles, and natural organic matters (NOMs), are ubiquitously present in environmental systems. Their estimated concentrations in the environment are in the range of 1–20 mg/L, which are typically several orders of magnitude higher than that of engineered nanoparticles (e.g., GO and carbon nanotubes) (Batley et al., 2013). Therefore, once released into the natural aquatic environment, the fate and transport of GO are expected to be greatly influenced by their heteroaggregation with natural colloids. Recently, much attention has been given on the heteroaggregation between GO and montmorillonite, kaolinite, or goethite (Huang et al., 2016; Sotirelis and Chrysikopoulos, 2016; Zhao et al., 2015), layered double hydroxides or oxides (Wang et al., 2017; Zou et al., 2016a; Zou et al., 2016b), SiO_2 (Chowdhury et al., 2014a), hematite (Feng et al., 2017), and Al_2O_3 (Chowdhury et al., 2014b; Ren et al., 2014). The results obtained from these studies revealed that surface charge and functional groups of the natural particles, as well as solution chemistry, could affect the heteroaggregation behavior of GO.

Sedimentation is also a crucial process affecting GO transport in aquatic to terrestrial environments (Quik et al., 2014). However, the sedimentation of GO has not been thoroughly investigated. Although heteroaggregation has been considered to be a vital process for the sedimentation of nanoparticles, the interdependence between heteroaggregation and sedimentation has not been well understood. Our previous study demonstrated that GO interacted favorably with the oppositely charged hematite colloids, leading to the sedimentation of hematite colloids (Feng et al., 2017). Nevertheless, natural aquatic environment is complex, and other factors, including NOMs, pH, and ionic strength, might influence the heteroaggregation and sedimentation behaviors of GO (Huynh et al., 2014; Quik et al., 2014; Wang et al., 2015a; Wang et al., 2015b; Zhao et al., 2015; Zhou et al., 2012). Therefore, in this study, the effects of these factors on interdependence of the heteroaggregation and sedimentation of GO with hematite nanoparticles (HemNP) were examined. Suwannee River humic acid (SRHA), alginate, and bovine serum albumin were respectively used here as representations of the humic substance, polysaccharide, and protein fractions of NOM to study the influences of these fractions on the heteroaggregation and sedimentation behaviors of GO. From experimental observations, the role of heteroaggregate sizes and zeta potentials on GO—HemNPs heteroaggregate sedimentation rates were elucidated.

In the natural aquatic environment, GO will be co-existed with environmental pollutants (Zhao et al., 2014). For example, that tetracycline is a popular antibiotic and could be present in the environment at concentrations up to 110 μg/L (Zhang et al., 2015). Due to the high adsorption capacities of GO, adsorption of co-existing pollutants on GO is likely to occur and thus influences the fate and toxicity of these contaminants (Hu et al., 2014; Kyzas et al., 2014; Li et al., 2013; Zhao et al., 2011). (Jiang et al., 2018; Sun et al., 2017)As the heteroaggregation of GO with natural colloids can possibly change the structures and properties of GO, this process is expected to affect GO adsorption ability for co-existing pollutants. Former studies found that heteroaggregation between GO and natural minerals (e.g., montmorillonite, kaolin, and goethite) or metal oxide particles (e.g., SiO_2 and Al_2O_3) greatly inhibited the adsorption of 17β-estradiol and bisphenol A on GO (Jiang et al., 2018; Sun et al., 2017). Therefore, the influence of heteroaggregation on the adsorption ability of GO toward tetracycline was also investigated in this study.

2. Experimental section

2.1. Preparation and characterization of GO and HemNPs

Well-dispersed water suspension of graphene oxide (>99% purity) was purchased from XFNANO Materials Tech Co. (Jiangsu, China). Based on the information provided by the supplier, the GO were produced by the modified Hummers method (Hummers and Offeman, 1958) with the flake size of 50–200 nm and the thickness of 0.8–1.2 nm. The properties of GO were extensively characterized using various techniques. In the GO stock suspension, total organic carbon content (TOC) and GO hydrodynamic diameters were determined through high temperature (1200 °C) catalytic oxidation (Vario TOC, Elementar, Germany) and dynamic light scattering (DLS) (Malvern Zetasizer Nano series Nano-ZS, MA, USA), respectively. Surface elemental compositions of GO were determined by X-ray photoelectron spectroscopy (XPS) (Perkin-Elmer PHI 550 ESCA/SAM, USA). GO UV–vis spectra analysis was performed on a Varian Cary 50 spectrophotometer (Varian, USA). Transmission electron microscopy (TEM) images of GO were collected on a JEM-200 CX (JEOL, Japan). In addition, Fourier transform infrared (FTIR, Vector-22 spectrometer, Bruker, Germany) and Raman spectra (Raman Senterra microscope, Bruker, Germany) of GO were also obtained.

Hematite nanoparticles (HemNPs, <50 nm) were purchased from Sigma Aldrich Co. (St. Louis, MO, USA). The stock suspensions of HemNPs were prepared by dispersing the nanoparticle powder into deionized (DI) water (18.2 mΩ·cm, Milli-Q, Millipore, USA). The concentrations of the HemNPs in stock suspensions were determined through gravimetric analysis. Detailed characterization results of GO and HemNPs can be found in Fig. S1 and Table S1 of the Supplementary Materials (SM).

2.2. Preparation of stock solutions

A NaCl stock solution was prepared with DI water and filtered through a 0.22-μm syringe filter (Millipore, MA). Suwannee River humic acid (SRHA) was obtained from International Humic Substances Society. Bovine serum albumin (BSA), sodium alginate, and tetracycline hydrochloride ($C_{22}H_{24}N_2O_8 \cdot HCl$, 99% purity) were purchased from Sigma-Aldrich (Shanghai, China). SRHA, BSA and alginate stock solutions were prepared by dissolving 5.0 mg macromolecules in 20 mL DI water. In the case of SRHA, the solution pH was adjusted to ca. 10 using NaOH to ensure that SRHA had completely dissolved. After

being stirred overnight, the mixtures were filtered through 0.22-μm membrane filters. The TOC values of these solutions were determined through a total carbon analyzer (Vario TOC, Elementar, Germany). Selected chemical and physical properties of these three NOMs are listed in SM Table S2. Their structures and surface groups were also characterized through FTIR and are presented in SM Fig. S2 and Table S3. Stock solution of tetracycline was prepared with DI water. All the stock solutions were stored in the dark at 4 °C.

2.3. Heteroaggregation and sedimentation experiments

The heteroaggregation experiments of GO and HemNPs were performed in 4-mL disposable cuvettes at 25 °C, pH 5.2 (pH of most natural waters = 5–9 (Organization WH, 1996)) and in the presence of 0.1 mM NaCl. At this solution chemistry, GO and HemNPs are stable to homoaggregation (Feng et al., 2017). For the experiments, GO concentration was 100 μg TOC/L and HemNP concentration was 10 mg/L, because the sedimentation rate at this specific GO/HemNP mass concentration ratio (0.01) was found to be the highest (optimal value, will be discussed later in the subsequent section). The change in hydrodynamic diameter (D_h) of the GO—HemNP heteroaggregates within 10 min of heteroaggregation were measured through time-resolved dynamic light scattering (DLS) with a 10 s of data accumulation for each reading. The light scattering system (Malvern Zetasizer Nano series Nano-ZS, MA, USA) was equipped with a 633-nm laser source and a 173° backscattering detector. A 10 min of time-resolved DLS measurement was employed here because the trend of change in aggregate size was easy to observe and such short duration is beneficial for experimental planning.

In sedimentation experiments, similar solution chemistry was used (pH 5.2 and 0.1 mM NaCl). The concentration of GO was varied in the range of 5–1500 μg/L, while concentration of HemNPs was fixed at 10 mg/L. The experiments were performed in 4.0-mL cuvettes and the suspension volumes were 3 mL. Before being placed into the spectrophotometer (Cary 50, Varian, USA), the nanoparticle suspensions were shaken vigorously (<10 s) to ensure their uniformity. The change in the absorbance of the aggregating suspensions during ca. 10–30 min of aggregation was recorded at 760 nm wavelength at 25 °C. It should be noted that the absorption of GO was negligible compared to that of HemNP at 760 nm (Feng et al., 2017). Initial sedimentation rates were obtained by performing linear regression analyses of the absorbance data recorded over the first 1 min of sedimentation. These experiments were at least duplicated at each GO/HemNP ratio. A HemNP concentration of 10 mg/L was used to ensure suitable scattered and transmitted light intensities for heteroaggregation experiments (DLS measurements) and sedimentation experiments (760 nm absorbance measurements), respectively.

To evaluate the influence of different NOMs on the heteroaggregation and sedimentation behaviors of GO and HemNPs, heteroaggregation and sedimentation experiments were also conducted in the presence of 0.005–50.0 mg TOC/L of SRHA, alginate, BSA. In these experiments, GO concentration was 100 μg/L and HemNP concentration was 10 mg/L (e.g, GO/HemNP mass concentration ratio = 0.01). NOMs are added into the aqueous phase right before the addition of GO and HemNPs. After 10 min of heteroaggregation, the size of the heteroaggregates was obtained using DLS. The sedimentation rates of GO and HemNPs in the presence of NOMs were also obtained using similar methods described above. Heteroaggregation and sedimentation experiments at this optimal GO/HemNP ratio were also conducted in different electrolyte concentrations (0.1 to 100 mM NaCl) to better reflect the actual environmental conditions.

2.4. Disaggregation experiments

In natural waters, pH would be gradually elevated to extreme levels due to the consumption of dissolved CO_2 in eutrophication (Turner and Chislock, 2010). Therefore, disaggregation of GO—HemNP heteroaggregates with gradually raising pH from 5.2 to 11.0 was explored in this study. In order to prepare for disaggregation experiments (in the absence of NOMs), GO—HemNP heteroaggregates were firstly formed for 10 min at pH 5.2 and 0.1 mM NaCl, and at the optimal GO/HemNP ratio of 0.01 (100 μg TOC/L GO and 10 mg/L HemNP). Afterward, solution pH was raised to 8.0 and the nanoparticles were allowed to undergo 10 min heteroaggregation/sedimentation. Finally, the pH was raised to 11.0 and this condition was also kept for 10 min. During pH adjustment, the GO—HemNP mixtures were manually shaken for 1 min. It was observed that this action did not affect the size of GO—HemNP heteroaggregates (SM Fig. S3).

2.5. Zeta potential measurements

The zeta potentials of the NPs at 25 °C at different condition of interest were determined using a Malvern Zetasizer Nano series Nano-ZS (MA, USA). After being prepared, the nanoparticle suspensions were promptly transferred to disposable folded capillary zeta cells. The measurements were then started after 30 s of temperature equilibration. The zeta-potentials were calculated by the Zetasizer Software (Version 7.10, MA, USA) based on Henry's function with Smoluchowski approximation. The measurements were conducted in triplicate at each condition.

2.6. Adsorption experiments

Tetracycline, a representative organic co-existing contaminant, was used to evaluate the impact of heteroaggregation on the adsorption ability of GO. Adsorption experiments were performed in 40-mL glass vials equipped with polytetrafluoroethylene (PTFE)-lined screw caps and incubated on a rotary shaker operating at 180 rpm and 25 °C. In these experiments, the concentration of GO was fixed at 20 mg/L, while the HemNP concentrations were varied from 0 to 2 g/L, which corresponded to HemNP/GO ratios of 0–100. For the experiments, 20-mL GO and HemNP suspensions were firstly mixed together at 0.1 mM NaCl and pH 5.5. After 30 min of heteroaggregation, predetermined volumes of tetracycline stock solution were added to the GO—HemNP mixtures to achieve initial concentrations of 5.0 mg/L. Then, the mixtures were left aside for 24 h (the tetracycline adsorption reached equilibrium at this duration, SM Fig. S4) and filtered through 0.22-μm membrane filters to remove nanoparticles and heteroaggregates. Afterward, the residual concentrations of tetracycline in the aqueous phase were determined at 355 nm by a spectrophotometer (Mapada 3200 UV–Vis, Shanghai, China). In these experiments, uncommonly high concentrations of GO, HemNPs, and tetracycline were used to ensure the adsorption of tetracycline could be discerned by a UV–Vis spectrophotometer.

3. Results and discussion

3.1. Heteroaggregation and sedimentation of GO with HemNPs

At pH 5.2 and 0.1 mM NaCl, HemNPs were found to be stable and no obvious homoaggregation were occurred at a concentration of 10 mg/L, as shown in Fig. 1a. The mixing of 10 mg/L HemNPs with 100 μg TOC/L GO resulted in the rapid increase of aggregate hydrodynamic diameters (Fig. 1a). This observation was indicative of GO—HemNP heteroaggregation through electrostatic attraction because GO is negatively charged and HemNP is positively charged (Fig. 1b) (Huynh et al., 2012; Rollie and Sundmacher, 2008). After 30 min of heteroaggregation, GO possibly neutralized HemNPs completely, as the zeta potentials of GO—HemNP heteroaggregates were close to neutral (Fig. 1b). The rapid heteroaggregation of GO and HemNPs also lead to the observable sedimentation of GO—HemNP heteroaggregates as presented in Fig. 1c.

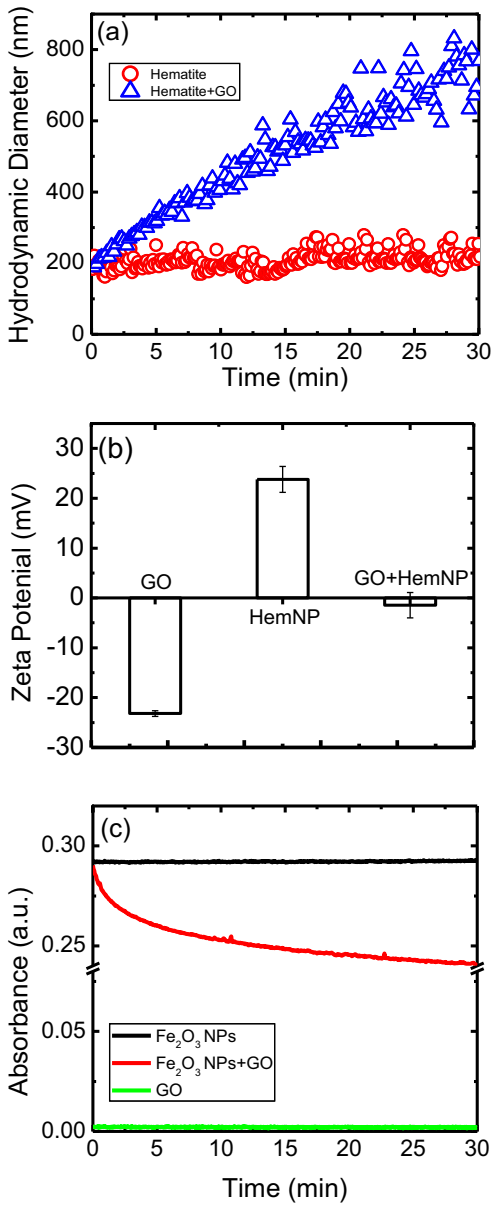

Fig. 1. (a) Representative HemNP homoaggregation and GO—HemNP heteroaggregation profiles, (b) zeta potential values, and (c) sedimentation profiles of GO, HemNP, and GO—HemNP heteroaggregates. The concentrations of HemNPs and GO were 10 mg/L and 100 μg TOC/L, respectively. The experiments were conducted at 0.1 mM NaCl and pH 5.2. In (b), the zeta potential measurements were started right after nanoparticle suspension preparation and 30 s of temperature equilibration. Error bars represent the standard deviations of at least three measurements.

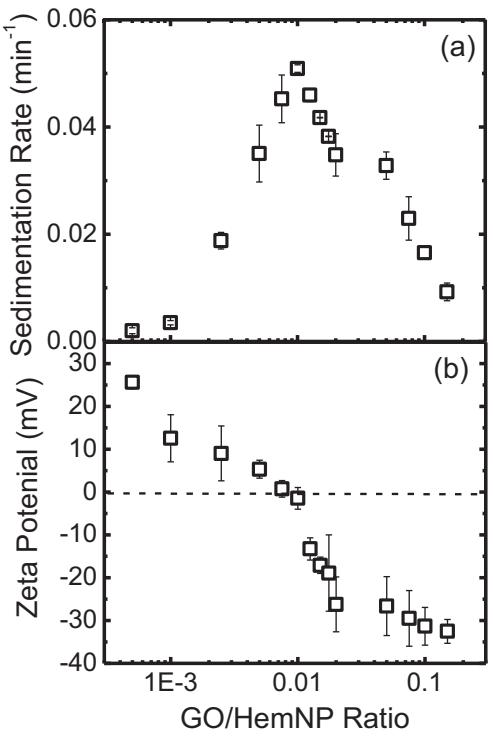

Fig. 2. (a) Sedimentation rates and (b) zeta potential values of heteroaggregates formed at various GO/HemNP ratios at 0.1 mM NaCl and pH 5.2. The concentration of HemNPs was 10 mg/L. The zeta potential measurements were started right after nanoparticle suspension preparation and 30 s of temperature equilibration. Error bars represent standard deviations of duplicate samples.

To better understand the heteroaggregation and sedimentation behaviors of GO with oppositely charged colloids, sedimentation of GO—HemNP mixtures under a wide range of GO/HemNP mass concentration ratios at 0.1 mM NaCl and pH 5.2 was investigated. Initial sedimentation rates at different GO/HemNP ratios that calculated from SM Fig. S5 are presented in Fig. 2a. It is apparent that the sedimentation rate of the GO—HemNP mixtures strongly depends on GO/HemNP mass concentration ratios. The sedimentation rates first increased, reached a maximum value, and then decreased with increasing GO/HemNP mass concentration ratios from 0 to 0.15. In the meantime, as the GO/HemNP mass concentration ratios increased, the zeta potentials of heteroaggregates gradually changed from positive to negative values (Fig. 2b). At the optimal GO/HemNP ratio of 0.01, GO—HemNP heteroaggregates had a maximum sedimentation rate of 0.053 min^{-1} and their charges were close to zero, as shown in Fig. 2b. Therefore, the attachment of GO on HemNP surfaces through electrostatic attraction, which then resulted in HemNP charge neutralization and reversal, are likely the main mechanism for the heteroaggregation and sedimentation of oppositely charged GO and HemNPs (Loosli and Stoll, 2012; Yates et al., 2005; Yi et al., 2015).

3.2. Effects of NOM and ionic strength on GO—HemNP heteroaggregation and sedimentation

Previous studies demonstrated that both GO and HemNPs had good adsorption capacity for typical NOMs, such as SRHA, alginate, and BSA (SM Table S4). Therefore, it is of interest to investigate the effects of NOM on the heteroaggregation and sedimentation of GO—HemNP aggregates. These experiments were performed in the presence 0.005–5.0 mg TOC/L NOM at pH 5.2 and 0.1 mM NaCl. The GO and HemNP concentrations were respectively fixed at 100 μg TOC/L and 10 mg/L, where the favorable sedimentation occurred (Fig. 2). Representative sedimentation profiles are presented in SM Fig. S6. It should be noted that the presence of these NOMs was found not to interfere with the DLS measurements of GO—HemNP mixtures in this study. Because NOMs were added into the aqueous phase before the addition of GO and HemNPs, it was likely that the nanoparticles were already coated NOMs before heteroaggregation took place. Since the concentrations of GO and HemNPs were fixed, the degree of NOM coating on the surface of nanoparticles possibly depended on NOM concentrations.

As shown in Fig. 3, the heteroaggregation and sedimentation of GO and HemNPs in the presence of SRHA and alginate were similar. Fig. 3a and b show that these NOMs greatly reduced the heteroaggregation and sedimentation of GO—HemNP mixtures. For instance, with a gradual increase of SRHA and alginate concentrations from 0 to 0.5 mg TOC/L, the hydrodynamic diameter of heteroaggregates measured after 10 min of heteroaggregation was only ca. 200 nm (~500 nm in the absence of SRHA and alginate) (Fig. 3a), while the sedimentation rates

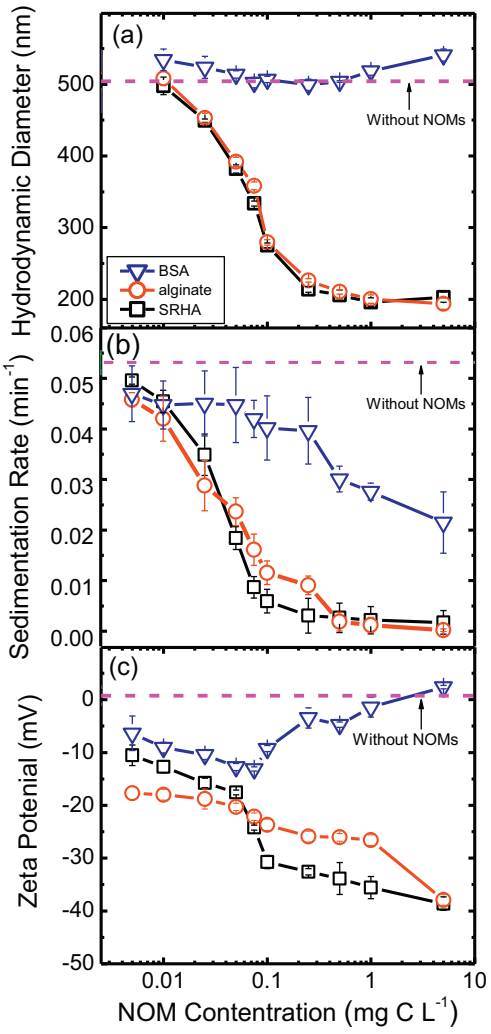

Fig. 3. (a) hydrodynamic diameters, (b) sedimentation rates, and (c) zeta potentials of GO—HemNP heteroaggregates at pH 5.2 and 0.1 mM NaCl in the presence of different NOMs. The concentrations of GO and HemNPs were 100 μg TOC/L and 10 mg/L, respectively. In (b), the hydrodynamic diameters were measured after 10 min of heteroaggregation. Error bars represent standard deviations of duplicate samples.

sharply decreased from 0.053 min^{-1} to zero (Fig. 3b). When SRHA and alginate concentrations were higher than 0.5 mg TOC/L, GO—HemNP heteroaggregation and sedimentation did not occur. Fig. 3c shows that the zeta potentials of GO—HemNP heteroaggregates became more negative as the concentrations of SRHA and alginate increased (e.g., from nearly zero to ca. −38 mV when SRHA and alginate concentrations were increased from 0 to 5 mg TOC/L).

BSA, on the other hand, had virtually no effect on GO—HemNP heteroaggregation and lower inhibition effect on the sedimentation of GO—HemNP aggregates compared to SRHA and alginate. Specially, the sedimentation rates reduced from 0.053 to only ca. 0.030 min^{-1} in the presence of 0.5 mg TOC/L BSA. Even with 5 mg TOC/L BSA, the GO—HemNP heteroaggregates still settled with a sedimentation rate of ca. 0.022 min^{-1} (Fig. 3b) and had a similar hydrodynamic diameter to the ones in the suspension without BSA (500–540 nm, Fig. 3a). The effect of BSA on the zeta potential of GO—HemNP heteroaggregates was also different from those of SRHA and alginate. Within the NOM concentration range of interest, the zeta potentials of the GO—HemNP heteroaggregates just slightly fluctuated and were close to neutral. This observation indicates the low stability of GO—HemNP heteroaggregates in BSA solution.

For better understanding of the effects of different NOMs on the heteroaggregation and sedimentation of GO and HemNPs (Fig. 3), the zeta potentials of GO (100 μg TOC/L) and HemNPs (10 mg/L) before and after the addition of different NOMs (1 mg/L) at pH 5.2 and 0.1 mM NaCl were further determined. The results are shown in SM Fig. S7. At pH 5.2, SRHA and alginate were negatively charged due to the deprotonation of the predominant carboxyl groups (SM Fig. S2 and Table S3). The adsorption of SRHA and alginate thus expectedly increased the negativity of GO surface charge (SM Fig. S7). However, such charge reduction was more pronounced in the presence of SRHA. Since alginate had twice the hydrodynamic diameter and half the zeta potential of SRHA (379 nm vs. 178 nm and – 25 mV vs. – 50 mV) (Loosli et al., 2013), these NOMs likely had similar charge densities. As a result, the lower zeta potentials of SRHA—GO than those of alginate—GO (SM Fig. S7) could be possibly explained by the higher degree of SRHA adsorption toward GO surfaces (SM Table S4). In the case of HemNPs, the adsorption of SRHA and alginate reversed their surface charge from positive to negative (SM Fig. S7), causing electrosteric repulsion toward GO (Huynh et al., 2012). Thus, the heteroaggregation and sedimentation of GO—HemNP aggregates decreased (Fig. 3a and b). When SRHA and alginate concentrations were increased, electrosteric repulsion between GO and HemNPs became stronger as more GO and HemNP surface was covered with NOMs. For that reason, higher level of reduction in GO—HemNP heteroaggregation and sedimentation was expected to occur in suspensions containing higher SRHA and alginate concentrations (Fig. 3).

BSA is a protein and contains many functional groups, including carboxyl and amide (SM Fig. S2 and Table S3). Because its isoelectric point is ca. pH 5 (Huangfu et al., 2013), BSA was neutrally charged under experimental condition (pH 5.2). The adsorption of neutral BSA macromolecules to the charged GO and HemNPs reduced the absolute surface charge values of these nanoparticles as presented in SM Fig. S7. It is shown in Fig. 3a that the size of GO—HemNP heteroaggregates slightly changed within the tested BSA range, while the corresponding sedimentation rates unexpectedly declined (Fig. 3b). As BSA concentration was increased, the number of nanoparticles present in the heteroaggregates was probably reduced. The coating BSA layer of GO and HemNP could lower the number of nanoparticle collision through the increase in steric repulsion and the decrease in electrostatic attraction (SM Fig. S6). Within the heteroaggregates, the reducing in hydrodynamic diameter via losing nanoparticles may counterbalance the increasing in hydrodynamic diameter via gaining BSA. This synergetic effect would possibly result in the nearly constant hydrodynamic diameters of heteroaggregates observed in the experiments with BSA (Fig. 3a). It is also reasonable to speculate that the densities of GO—HemNP heteroaggregates were smaller at higher BSA concentrations, resulting in the reduction in sedimentation rate (Fig. 3b). This hypothesis could be verified by determining GO—HemNP heteroaggregate fractal dimensions at different BSA concentrations. However, this investigation is out of the scope of this study and could be performed in the future. After all, the presence of steric repulsive interaction, together with the decrease in electrostatic attraction was likely the mechanisms reducing the sedimentation of GO—HemNP aggregates in BSA solutions (Huangfu et al., 2013; Sheng et al., 2016). In the case of SRHA and alginate, it is reminded that the reason for reducing in GO—HemNP heteroaggregation and sedimentation was the presence of electrosteric repulsive interaction.

Effects of ionic strength on the sedimentation of GO (100 μg TOC/L) and HemNPs (10 mg/L) at pH 5.2 were also investigated to better understand the behaviors of these nanoparticles in the natural environment. As shown in Fig. 4a, the sedimentation of the GO—HemNP mixtures increased from 0.05 to 0.37 min^{-1} when NaCl concentration was varied from 0.1 to 100 mM. Due to the increased electrostatic screening at elevated ionic strengths (Afrooz et al., 2013), GO and HemNPs were expected to undergo both heteroaggregation and homoaggregation, and the latter was possibly the dominant aggregation mechanism. Nevertheless, this combination was expected to enhance the whole aggregation process, resulting in the formation of large

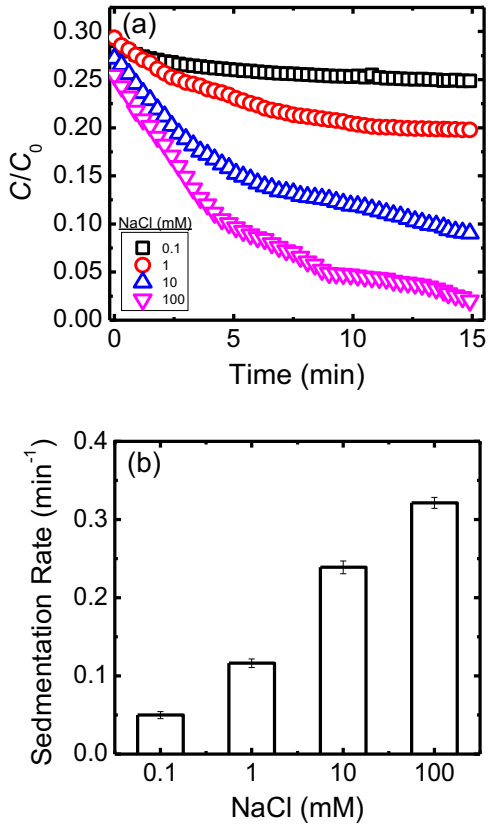

Fig. 4. (a) Sedimentation kinetics and (b) sedimentation rate of GO/HemNP heteroaggregates at pH 5.2 in the presence of different concentrations of NaCl. Experiments were performed at HemNP concentration of 10 mg/L and GO concentration of 100 μg TOC/L.

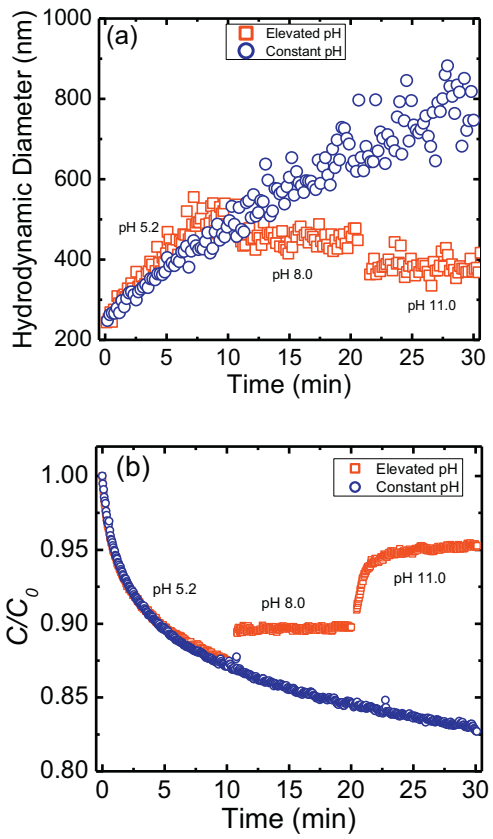

Fig. 5. (a) Aggregation and disaggregation profiles of GO/HemNP heteroaggregates, (b) sedimentation kinetics at 0.1 mM NaCl with the increase in pH from 5.2 to 8.0 and 11.0. The concentrations of HemNPs and GO were 10 mg/L and 100 μg TOC/L, respectively.

aggregates and therefore rapid sedimentation of nanoparticles under high ionic strengths.

3.3. Disaggregation of GO—HemNP heteroaggregates at elevated pH

The disaggregation of nanoparticle aggregates could occur in the environments having solution chemistry favorable for repulsive interaction, such as high pH (Huynh and Chen, 2014). This phenomenon would affect the sedimentation and transport of GO and HemNPs in aquatic systems. Therefore, further heteroaggregation and sedimentation experiments were conducted to investigate the behaviors of GO—HemNP heteroaggregates in this scenario. For the experiments, the heteroaggregates were firstly formed for 10 min at an optimal GO/HemNP ratio of 0.01 at pH 5.2, 0.1 mM NaCl. Then, the solution pH was stepwise raised to 8.0 for 10 min and 11.0 for another 10 min. Heteroaggregation and sedimentation profiles of these experiments are presented in Fig. 5. As shown in Fig. 5a, increasing of pH stopped heteroaggregation, and eventually led to a reduction of heteroaggregate size (i.e., from ~500 nm (pH 5.2) to ~450 nm (pH 8.0) and ~380 nm (pH 11.0)), possibly due to the increase in electrostatic repulsion of GO and HemNPs at high solution pH. The disaggregation was observed to have a strong influence on GO—HemNP sedimentation (Fig. 5b). Specifically, the sedimentation was halted during 10 min at pH 8.0. At pH 11.0, disaggregation took place and the detached particles/fragments diffused back to the supernatant.

SM Fig. S8 shows that as pH was increased, the surface charge of GO became more negative due to more deprotonation of carboxyl, enolic, and phenolic groups (Szabó et al., 2006; Wu et al., 2013), while that of HemNP would be reversed from positive to negative. Charge reversal of HemNP decreased the electrostatic attraction and increased electrostatic repulsion in GO—HemNP mixtures. Therefore, the energy barrier between GO and HemNP was increased, thus weakened GO—HemNP bonds and resulted in the detachment of particles within the heteroaggregates (Huynh and Chen, 2014). Nevertheless, the uncompleted disaggregation of the heteroaggregates indicates that GO—HemNP heteroaggregates cannot be completely separated through diffusion (Yi et al., 2015).

3.4. Adsorption of tetracycline by GO—HemNP heteroaggregates

It can be seen from Fig. 6 that GO had great adsorption capacity for tetracycline and the amount of tetracycline adsorbed decreased with the increase in HemNP concentration. For instance, ca. 80% of tetracycline (initial concentration = 5 mg/L) was removed solely by 20 mg/L GO after 24 h. This result was in agreement with the study of Gao and co-authors (Gao et al., 2012). However, virtually no tetracycline adsorption occurred when the HemNP concentration was higher than 100 mg/L (GO/HemNP ratio <0.2) (Fig. 6).

Because tetracycline is likely to be positively or neutrally charged at pH 5.2 (Gao et al., 2012), its adsorption on GO surface (negatively charged) was expected to be more favorable than that on HemNP surface (positively charged). In addition, tetracycline contains four aromatic rings with various functional groups on each ring, including amino, carboxyl, phenol, alcohol, and ketone. Therefore, it is possibly easier for tetracycline to be adsorbed on GO through π–π stacking than to HemNP surface. However, this reason was still not enough to explain the phenomenon observed in Fig. 6. From Fig. 2b, it is noted that the zeta potentials of GO—HemNP heteroaggregates became less negative, zero, and more positive GO/HemNP ratio was decreased from 0.1 to 0.01. Therefore, the adsorption of tetracycline to GO—HemNP heteroaggregates is speculated to be more difficult at lower GO/

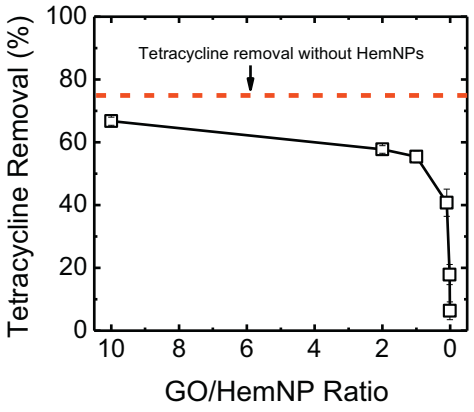

Fig. 6. Adsorption removal of tetracycline by GO–HemNP mixtures at different HemNP concentrations. GO concentration = 20 mg/L, tetracycline concentration = 5 mg/L, NaCl = 0.1 mM, and pH = 5.2.

HemNP ratios due to the reduction in electrostatic attraction between tetracycline and these heteroaggregates.

To elucidate other mechanism causing the declining of tetracycline adsorption at low GO/HemNP ratios, the conformation of GO—HemNP heteroaggregates formed when HemNP mass concentration greatly exceeds that of GO (GO/HemNP ratio = 0.004) was observed under a TEM. SM Fig. S9 shows that GO surface was almost completely covered by HemNPs. This finding indicated that the adsorption sites of GO were possibly blocked when these nanosheets underwent heteroaggregation with HemNPs. Therefore, more adsorption sites on GO surfaces would not be available for tetracycline adsorption at higher HemNP mass concentrations.

4. Conclusions and environmental implications

This study systemically investigated the interdependence of heteroaggregation and sedimentation behaviors of GO with natural colloids. Experimental results showed that GO favorably undergo heteroaggregation with the oppositely charged HemNP due to electrostatic attraction. The heteroaggregation then lead to a rapid sedimentation of the GO—HemNP mixtures. The sedimentation rate of the GO—HemNP mixtures highly depended on GO/HemNP mass concentration ratios. At the optimal GO/HemNP ratio of 0.01, where the surface charges of heteroaggregates were close to zero, GO—HemNP undergo fast heteroaggregation and had a maximum sedimentation rate of 0.053 min^{-1}. Based on that information, GO is less likely to suspend and transport over a long distance in the hematite enrichment aquatic environment. However, the favorable interaction between GO and hematite can be greatly inhibited by the presence of naturally occurring NOM such as humic substances (SRHA), polysaccharide (alginate), and protein (BSA). Therefore, the mobility of GO in surface waters is likely to be greatly enhanced. In addition, GO mobility is found to increase, due to disaggregation, when GO heteroaggregates enters environments having elevated solution pH.

Because GO heteroaggregation has been found to greatly affect the adsorption of co-existing contaminants, they should be included in models predicting the fate and transport of these contaminants in GO-contaminated environments. Specifically, at environmentally relevant condition (pH 5.5 and 0.1 mM NaCl), the adsorption of tetracycline (p*Ka* = 3.3, 7.7, and 9.7, (Gao et al., 2012)) on GO decreased due to the blocking of GO as GO and HemNPs underwent heteroaggregation. Similar blocking mechanism is also expected for the adsorption of non-ionic co-existing contaminants with higher hydrophobicity on GO in the presence of HemNPs. In the case of ionic co-existing contaminants (e.g., heavy metals), they can interact with both GO and HemNPs through various processes, such as charge screening and neutralization, and hydrophilic interactions. Further studies on the behaviors of these contaminants in the occurrence of GO—HemNP heteroaggregation and sedimentation are therefore required. Moreover, it can be concluded from this study that the use of GO for removing co-existing contaminants might not be applicable in systems where oppositely charged colloids are abundant.

Acknowledgments

This work was supported by the National Natural Science Foundation of China (21707019), the Characteristic Innovation Project of High Education Department of Guangdong Province (2017KTSCX058), the Science and Technology Planning Project of Guangzhou City (201804010396), and the Science and Technology Planning Project of Guangdong Province (2017A050506052, 2017A020216010, and 2017B020216003). Y. F. acknowledges her newborn son and daughter, Ze-Han Jin and Ze-Xi Jin, for the joy bring from them.

Appendix A. Supplementary data

Additional details on the characterization of GO, together with data on the heteroaggregation, sedimentation, and zeta potential measurements of GO—HemNP mixtures at different conditions. Supplementary data associated with this article can be found in the online version, at doi: https://doi.org/10.1016/j.scitotenv.2018.08.046.

References

Afrooz, A.R.M.N., Khan, I.A., Hussain, S.M., Saleh, N.B., 2013. Mechanistic heteroaggregation of gold nanoparticles in a wide range of solution chemistry. Environ. Sci. Technol. 47, 1853–1860.
Akhavan, O., Ghaderi, E., 2010. Toxicity of graphene and graphene oxide nanowalls against bacteria. ACS Nano 4, 5731–5736.
Batley, G.E., Kirby, J.K., McLaughlin, M.J., 2013. Fate and risks of nanomaterials in aquatic and terrestrial environments. Acc. Chem. Res. 46, 854–862.
Bianco, A., 2013. Graphene: safe or toxic? The two faces of the medal. Angew. Chem. Int. Ed. 52, 4986–4997.
Chang, Y.L., Yang, S.T., Liu, J.H., Dong, E., Wang, Y.W., Cao, A.N., et al., 2011. In vitro toxicity evaluation of graphene oxide on A549 cells. Toxicol. Lett. 200, 201–210.
Chowdhury, I., Duch, M.C., Mansukhani, N.D., Hersam, M.C., Bouchard, D., 2014a. Deposition and release of graphene oxide nanomaterials using a quartz crystal microbalance. Environ. Sci. Technol. 48, 961–969.
Chowdhury, I., Duch, M.C., Mansukhani, N.D., Hersam, M.C., Bouchard, D., 2014b. Interactions of graphene oxide nanomaterials with natural organic matter and metal oxide surfaces. Environ. Sci. Technol. 48, 9382–9390.
Feng, Y., Liu, X., Huynh, K.A., McCaffery, J.M., Mao, L., Gao, S., et al., 2017. Heteroaggregation of graphene oxide with nanometer-and micrometer-sized hematite colloids: influence on nanohybrid aggregation and microparticle sedimentation. Environ. Sci. Technol. 51, 6821–6828.
Gao, Y., Li, Y., Zhang, L., Huang, H., Hu, J.J., Shah, S.M., et al., 2012. Adsorption and removal of tetracycline antibiotics from aqueous solution by graphene oxide. J. Colloid Interface Sci. 368, 540–546.
He, H.Y., Klinowski, J., Forster, M., Lerf, A., 1998. A new structural model for graphite oxide. Chem. Phys. Lett. 287, 53–56.
Hu, X.G., Kang, J., Lu, K.C., Zhou, R.R., Mu, L., Zhou, Q.X., 2014. Graphene oxide amplifies the phytotoxicity of arsenic in wheat. Sci. Rep. 4.
Huang, G.X., Guo, H.Y., Zhao, J., Liu, Y.H., Xing, B.S., 2016. Effect of co-existing kaolinite and goethite on the aggregation of graphene oxide in the aquatic environment. Water Res. 102, 313–320.
Huangfu, X.L., Jiang, J., Ma, J., Liu, Y.Z., Yang, J., 2013. Aggregation kinetics of manganese dioxide colloids in aqueous solution: influence of humic substances and biomacromolecules. Environ. Sci. Technol. 47, 10285–10292.
Hummers, W.S., Offeman, R.E., 1958. Preparation of graphitic oxide. J. Am. Chem. Soc. 80, 1339.
Huynh, K.A., Chen, K.L., 2014. Disaggregation of heteroaggregates composed of multiwalled carbon nanotubes and hematite nanoparticles. Environ. Sci.: Processes Impacts 16, 1371–1378.
Huynh, K.A., McCaffery, J.M., Chen, K.L., 2012. Heteroaggregation of multiwalled carbon nanotubes and hematite nanoparticles: rates and mechanisms. Environ. Sci. Technol. 46, 5912–5920.
Huynh, K.A., McCaffery, J.M., Chen, K.L., 2014. Heteroaggregation reduces antimicrobial activity of silver nanoparticles: evidence for nanoparticle–cell proximity effects. Environ. Sci. Technol. Lett. 1, 361–366.
Jiang, L.H., Liu, Y.G., Zeng, G.M., Liu, S.B., Que, W., Li, J., et al., 2018. Adsorption of 17 beta-estradiol by graphene oxide: effect of heteroaggregation with inorganic nanoparticles. Chem. Eng. J. 343, 371–378.

Kim, J., Cote, L.J., Huang, J.X., 2012. Two dimensional soft material: new faces of graphene oxide. Acc. Chem. Res. 45, 1356–1364.
Kyzas, G.Z., Deliyanni, E.A., Matis, K.A., 2014. Graphene oxide and its application as an adsorbent for wastewater treatment. J. Chem. Technol. Biotechnol. 89, 196–205.
Li, S.B., Irin, F., Atore, F.O., Green, M.J., Canas-Carrell, J.E., 2013. Determination of multi-walled carbon nanotube bioaccumulation in earthworms measured by a microwave-based detection technique. Sci. Total Environ. 445, 9–13.
Liao, K.H., Lin, Y.S., Macosko, C.W., Haynes, C.L., 2011. Cytotoxicity of graphene oxide and graphene in human erythrocytes and skin fibroblasts. ACS Appl. Mater. Interfaces 3, 2607–2615.
Liu, S.B., Zeng, T.H., Hofmann, M., Burcombe, E., Wei, J., Jiang, R.R., et al., 2011. Antibacterial activity of graphite, graphite oxide, graphene oxide, and reduced graphene oxide: membrane and oxidative stress. ACS Nano 5, 6971–6980.
Loosli, F., Stoll, S., 2012. Adsorption of TiO_2 nanoparticles at the surface of micron-sized latex particles. pH and concentration effects on suspension stability. J. Colloid Sci. Biotechnol. 1, 113–121.
Loosli, F., Le Coustumer, P., Stoll, S., 2013. TiO_2 nanoparticles aggregation and disaggregation in presence of alginate and Suwannee River humic acids. pH and concentration effects on nanoparticle stability. Water Res. 47, 6052–6063.
Organization WH, 1996. Guidelines for drinking water quality. Health Criteria and Other Supporting Information, 2nd edn. Vol 2. World Health Organization, Geneva.
Quik, J.T.K., Velzeboer, I., Wouterse, M., Koelmans, A.A., van de Meent, D., 2014. Heteroaggregation and sedimentation rates for nanomaterials in natural waters. Water Res. 48, 269–279.
Ren, X.M., Li, J.X., Tan, X.L., Shi, W.Q., Chen, C.L., Shao, D.D., et al., 2014. Impact of Al_2O_3 on the aggregation and deposition of graphene oxide. Environ. Sci. Technol. 48, 5493–5500.
Rollie, S., Sundmacher, K., 2008. Determination of cluster composition in heteroaggregation of binary particle systems by flow cytometry. Langmuir 24, 13348–13358.
Sheng, A.X., Liu, F., Xie, N., Liu, J., 2016. Impact of proteins on aggregation kinetics and adsorption ability of hematite nanoparticles in aqueous dispersions. Environ. Sci. Technol. 50, 2228–2235.
Sotirelis, N.P., Chrysikopoulos, C.V., 2016. Heteroaggregation of graphene oxide nanoparticles and kaolinite colloids. Sci. Total Environ. 579, 736–744.
Sun, W.L., Wang, C.H., Pan, W.Y., Li, S., Chen, B., 2017. Effects of natural minerals on the adsorption of 17 beta-estradiol and bisphenol A on graphene oxide and reduced graphene oxide. Environ. Sci.: Nano 4, 1377–1388.
Szabó, T., Tombácz, E., Illés, E., Dékány, I., 2006. Enhanced acidity and pH-dependent surface charge characterization of successively oxidized graphite oxides. Carbon 44, 537–545.
Tang, Y.L., Tian, J.L., Li, S.Y., Xue, C.H., Xue, Z.H., Yin, D.Q., et al., 2015. Combined effects of graphene oxide and Cd on the photosynthetic capacity and survival of *Microcystis aeruginosa*. Sci. Total Environ. 532, 154–161.
Turner, A.M., Chislock, M.F., 2010. Blinded by the stink: nutrient enrichment impairs the perception of predation risk by freshwater snails. Ecol. Appl. 20, 2089–2095.
Wang, H., Adeleye, A.S., Huang, Y., Li, F., Keller, A.A., 2015a. Heteroaggregation of nanoparticles with biocolloids and geocolloids. Adv. Colloid Interf. Sci. 226, 24–36.
Wang, H.T., Dong, Y.N., Zhu, M., Li, X., Keller, A.A., Wang, T., et al., 2015b. Heteroaggregation of engineered nanoparticles and kaolin clays in aqueous environments. Water Res. 80, 130–138.
Wang, J., Li, Y., Chen, W., Peng, J., Hu, J., Chen, Z., et al., 2017. The rapid coagulation of graphene oxide on La-doped layered double hydroxides. Chem. Eng. J. 309, 445–453.
Wu, L., Liu, L., Gao, B., Munoz-Carpena, R., Zhang, M., Chen, H., et al., 2013. Aggregation kinetics of graphene oxides in aqueous solutions: experiments, mechanisms, and modeling. Langmuir 29, 15174–15181.
Yang, K., Zhang, S.A., Zhang, G.X., Sun, X.M., Lee, S.T., Liu, Z.A., 2010. Graphene in mice: ultrahigh in vivo tumor uptake and efficient photothermal therapy. Nano Lett. 10, 3318–3323.
Yang, K., Li, Y.J., Tan, X.F., Peng, R., Liu, Z., 2013. Behavior and toxicity of graphene and its functionalized derivatives in biological systems. Small 9, 1492–1503.
Yates, P.D., Franks, G.V., Biggs, S., Jameson, G.J., 2005. Heteroaggregation with nanoparticles: effect of particle size ratio on optimum particle dose. Colloids Surf. A Physicochem. Eng. Asp. 255, 85–90.
Yi, P., Pignatello, J.J., Uchimiya, M., White, J.C., 2015. Heteroaggregation of cerium oxide nanoparticles and nanoparticles of pyrolyzed biomass. Environ. Sci. Technol. 49, 13294–13303.
Zhang, X.P., Liu, D., Yang, L., Zhou, L.M., You, T.Y., 2015. Self-assembled three-dimensional graphene-based materials for dye adsorption and catalysis. J. Mater. Chem. A 3, 10031–10037.
Zhao, G.X., Li, J.X., Ren, X.M., Chen, C.L., Wang, X.K., 2011. Few-layered graphene oxide nanosheets as superior sorbents for heavy metal ion pollution management. Environ. Sci. Technol. 45, 10454–10462.
Zhao, J., Wang, Z.Y., White, J.C., Xing, B.S., 2014. Graphene in the aquatic environment: Adsorption, dispersion, toxicity and transformation. Environ. Sci. Technol. 48, 9995–10009.
Zhao, J., Liu, F.F., Wang, Z.Y., Cao, X.S., Xing, B.S., 2015. Heteroaggregation of graphene oxide with minerals in aqueous phase. Environ. Sci. Technol. 49, 2849–2857.
Zhou, D.X., Abdel-Fattah, A.I., Keller, A.A., 2012. Clay particles destabilize engineered nanoparticles in aqueous environments. Environ. Sci. Technol. 46, 7520–7526.
Zhu, Y.W., Murali, S., Cai, W.W., Li, X.S., Suk, J.W., Potts, J.R., et al., 2010. Graphene and graphene oxide: Synthesis, properties, and applications. Adv. Mater. 22, 5226.
Zou, Y., Wang, X., Ai, Y., Liu, Y., Li, J., Ji, Y., et al., 2016a. Coagulation behavior of graphene oxide on nanocrystallined mg/al layered double hydroxides: batch experimental and theoretical calculation study. Environ. Sci. Technol. 50, 3658–3667.
Zou, Y., Wang, X., Chen, Z., Yao, W., Ai, Y., Liu, Y., et al., 2016b. Superior coagulation of graphene oxides on nanoscale layered double hydroxides and layered double oxides. Environ. Pollut. 219, 107–117.